CALPHAD: Computer Coupling of Phase Diagrams and Thermochemistry 50 (2015) 134–143

Contents lists available at ScienceDirect

CALPHAD: Computer Coupling of Phase Diagrams and Thermochemistry

journal homepage: www.elsevier.com/locate/calphad

Thermodynamic modeling of Cr–Nb and Zr–Cr with extension to the ternary Zr–Nb–Cr system

Hai-Jin Lu [a], Wen-Bo Wang [a], Nan Zou [a], Jian-Yun Shen [b], Xiao-Gang Lu [a,*], Yan-Lin He [a]

[a] School of Materials Science and Engineering, Shanghai University, Shanghai 200072, China
[b] General Research Institute for Non-ferrous Metals of Beijing, Beijing 100088, China

ARTICLE INFO

Article history:
Received 4 April 2015
Received in revised form
10 June 2015
Accepted 11 June 2015
Available online 23 June 2015

Keywords:
First-principles calculations
CALPHAD

ABSTRACT

The total energies of Laves phases in the Cr–Nb and Zr–Cr systems have been calculated by the pseudo-potential VASP code with a full relaxation of all structural parameters. The special quasirandom structures (SQSs) have been constructed and their total energies have been calculated by the VASP code to predict the enthalpies of mixing for bcc and hcp solid solution phases. The phonon calculations for the C14 and C15 Laves phases have been performed to analyze the phase stability at elevated temperatures. The experimental study on the Zr–Cr system has been carried out at different temperatures to determine the phase boundaries. Based on these results, thermodynamic models of Cr–Nb and Zr–Cr with extension to the ternary Zr–Nb–Cr systems have been developed in this work by using the CALPHAD approach.

© 2015 Elsevier Ltd. All rights reserved.

1. Introduction

Zirconium alloys are widely used in nuclear industry as cladding and structural materials in nuclear reactors for their excellent neutron economy, mechanic properties and corrosion resistance [1,2]. New generation of the Nb-containing Zr-based alloys has been developed to meet the requirement of high burnup of the nuclear fuel, such as Zirlo, E365, M5 [3], in which Cr is a trace element. In zirconium alloys, the Laves phases crystallize in the cubic ($MgCu_2$, C15) or hexagonal ($MgZn_2$, C14 and $MgNi_2$, C36) structures. The composition, size and distribution of the Laves phases precipitating in the zirconium alloys have a great influence on the final properties. Knowledge on thermodynamics is critical in studying the stability of phases including the Laves phases. However, report on the thermodynamic properties of Zr-base systems is comparatively defective and even contradictory.

The CALPHAD (CALculation of PHAse Diagram) approach [4,5] is a mature method for studying the thermodynamics and phase diagrams of the multi-components alloys. The thermodynamic properties and phase stability of a system can be calculated from the models describing the Gibbs energies of individual phases. The models contain adjustable parameters, which can be evaluated from the experimental data as well as the first-principles calculations providing much-needed thermochemical data, such as enthalpy of formation, entropy, heat capacity and so on.

In the present work, we calculated the total energies of end-member compounds for three Laves phase structures and solution phases for the Zr–Nb–Cr system at 0 K. The finite-temperature properties were obtained by performing the phonon calculations. These thermochemical data give physically-sound values for the Laves phases. Coupled with the first-principles calculations, key experiments and the CALPHAD method, we reassessed the Cr–Nb and Zr–Cr with extension to the ternary Zr–Nb–Cr system in order to obtain a physically-sound thermodynamic description, based on which the reliable extrapolation to multi-component systems is conceivable.

2. Experimental procedure

Two alloys were selected with the compositions of 20 at% and 60 at% Zr in the Zr–Cr system to determine the phase boundaries of C15/bcc Cr and C15/bcc Zr. The raw materials were 99.99 wt% Cr and 99.95 wt% Zr of nuclear purity from State Nuclear Baoti Zirconium Industry Company. Two ingots were prepared by arc melting under pure Ar atmosphere. Each sample was melted at least four times to get a homogeneous composition.

Each ingot was cut into several pieces, then the samples were sealed in clean silica glass tubes in a high purity argon atmosphere and annealed at 1273 K, 1373 K, 1473 K and 1573 K for 20, 10, 5 and 2 days, respectively. The annealing time was comparatively long to ensure the equilibrium of the phases. The samples were quenched by water at room temperature after heat treatments to keep the

* Corresponding author.
E-mail address: xglu@shu.edu.cn (X.-G. Lu).

http://dx.doi.org/10.1016/j.calphad.2015.06.002
0364-5916/© 2015 Elsevier Ltd. All rights reserved.

high-temperature microstructures. Then the samples were polished by standard metallographic techniques. The microstructures and compositions of all samples were obtained by electron probe microanalysis (EPMA) on JEOL JXA-8800R.

Table 1
EPMA results for the Zr–Cr alloys.

Alloys	Experimental condition	Phases	Measured composition (at% Zr)
Cr–60 at% Zr	1473 K/5d	C15	34.42
		bcc Zr	97.52
	1273 K/10d	C15	34.37
		bcc Zr	97.11
Cr–20 at% Zr	1573 K/2d	C15	30.05
		bcc Cr	1.29
	1473 K/5d	C15	33.76
		bcc Cr	1.92
	1373 K/20d	C15	32.63
		bcc Cr	1.06
	1273 K/10d	C15	33.07
		bcc Cr	1.07

3. Theoretical methodology

3.1. Ground state calculations

In the present work, the electronic structure calculations were performed within the framework of the density functional theory (DFT) by using the pseudo-potential method [6] incorporated into the Vienna *Ab initio* Simulation Package (VASP) code [7,8]. The standard projected augmented wave (PAW) potential [9] provided with VASP were used, and the Perdew–Wang version of the generalized gradient approximation (GGA-PW91) [10] was adopted. The total energies and the lattice parameters of all end-member compounds modeling three Laves structures as well as the elemental metals in their stable structures at 0 K were calculated. The plane wave energy cutoff of 400 eV was used throughout the present work. The k-point mesh of 16*16*16 was used for C15 structure by using the Monkhorst–Pack scheme, and a gamma mesh of 16*16*10 was used for the C14 and C36 structures. The volume of each structure was initially relaxed, followed by ionic and shape relaxations. The magnetic parameter for ferromagnetism was set throughout the calculations. ZenGen script-tool was

Table 2
Comparison of enthalpies of formation of the stoichiometric Laves phases in the Zr–Nb–Cr system.

Laves structures	Enthalpies of formation (kJ/mol)[a]	Lattice parameter, a/c (Å)	Method	Reference
C15–$NbCr_2$	−4.16	6.94	Pseudo-potential (VASP)	Present work
	−1.83	6.96	ADF-BAND	[30]
	−3.31	6.93	Pseudo-potential (VASP)	[28]
	−7.03	6.82	FLAPW	[35]
	−2.31	6.93	FLAPW	[36]
	−2.10	6.94	FP-LAPW	[37]
	−7.03	…	LMTO	[38]
	−7.06	…	Experiment	[25]
	…	6.97	Experiment	[34]
C15–$CrNb_2$	71.12	7.45	Pseudo-potential (VASP)	Present work
C15–$NbNb_2$	16.33	7.67	Pseudo-potential (VASP)	Present work
C15–$CrCr_2$	26.46	6.60	Pseudo-potential (VASP)	Present work
C15–$ZrCr_2$	−4.66	7.13	Pseudo-potential (VASP)	Present work
	−2.88	7.12	Pseudo-potential (VASP)	[47]
	−9.63	7.13	APW-lo	[48]
	…	7.21	Experiment	[42]
C15–$CrZr_2$	101.03	7.86	Pseudo-potential (VASP)	Present work
C15–$ZrZr_2$	27.05	8.26	Pseudo-potential (VASP)	Present work
C15–$NbZr_2$	48.37	8.03	Pseudo-potential (VASP)	Present work
C15–$ZrNb_2$	4.63	7.85	Pseudo-potential (VASP)	Present work
C14–$NbCr_2$	−2.58	4.89/8.07	Pseudo-potential (VASP)	Present work
	−1.81	4.88/8.06	Pseudo-potential (VASP)	[28]
	−1.83	4.83/7.87	FLAPW	[35]
	…	4.93/8.12	Experiment	[34]
C14–$CrNb_2$	7.23	5.36/8.32	Pseudo-potential (VASP)	Present work
C14–$NbNb_2$	15.51	5.48/8.66	Pseudo-potential (VASP)	Present work
C14–$CrCr_2$	27.78	4.66/7.67	Pseudo-potential (VASP)	Present work
C14–$ZrCr_2$	−3.02	5.09/8.08	Pseudo-potential (VASP)	Present work
	−1.27	5.08/8.07	Pseudo-potential (VASP)	[47]
	…	5.10/8.27	Experiment	[49]
C14–$CrZr_2$	93.06	5.69/8.44	Pseudo-potential (VASP)	Present work
C14–$ZrZr_2$	20.80	5.80/9.54	Pseudo-potential (VASP)	Present work
C14–$NbZr_2$	41.15	5.68/9.14	Pseudo-potential (VASP)	Present work
C14–$ZrNb_2$	1.61	5.59/8.92	Pseudo-potential (VASP)	Present work
C36–$ZrCr_2$	−3.94	5.06/16.37	Pseudo-potential (VASP)	Present work
	−2.14	5.05/16.33	Pseudo-potential (VASP)	[47]
	…	5.10/16.61	Experiment	[42]
C36–$CrNb_2$	72.14	5.36/17.30	Pseudo-potential (VASP)	Present work
C36–$NbCr_2$	−3.51	4.90/16.03	Pseudo-potential (VASP)	Present work
C36–$NbNb_2$	16.11	5.46/17.47	Pseudo-potential (VASP)	Present work
C36–$CrCr_2$	25.95	4.67/15.28	Pseudo-potential (VASP)	Present work
C36–$CrZr_2$	76.07	5.67/17.22	Pseudo-potential (VASP)	Present work
C36–$ZrZr_2$	23.07	5.81/19.11	Pseudo-potential (VASP)	Present work
C36–$NbZr_2$	43.77	5.70/18.29	Pseudo-potential (VASP)	Present work
C36–$ZrNb_2$	3.33	5.59/17.89	Pseudo-potential (VASP)	Present work

[a] The reference states are bcc Nb, bcc Cr and hcp Zr.

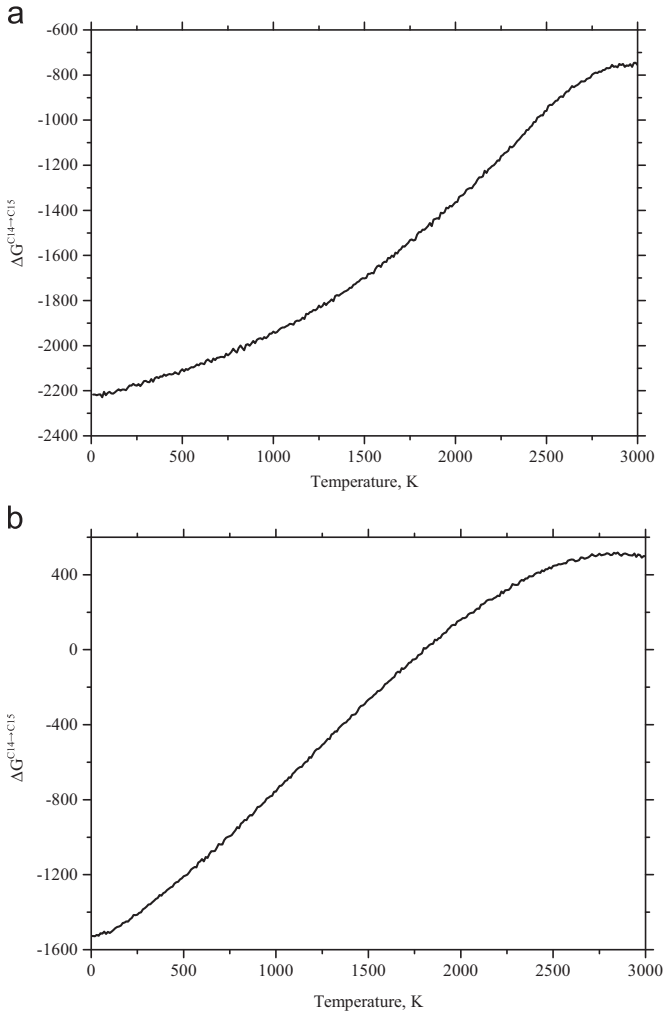

Fig. 1. Comparison of the calculated Gibbs energy difference between C15 and C14 in the Cr–Nb (a) and Zr–Cr (b) systems.

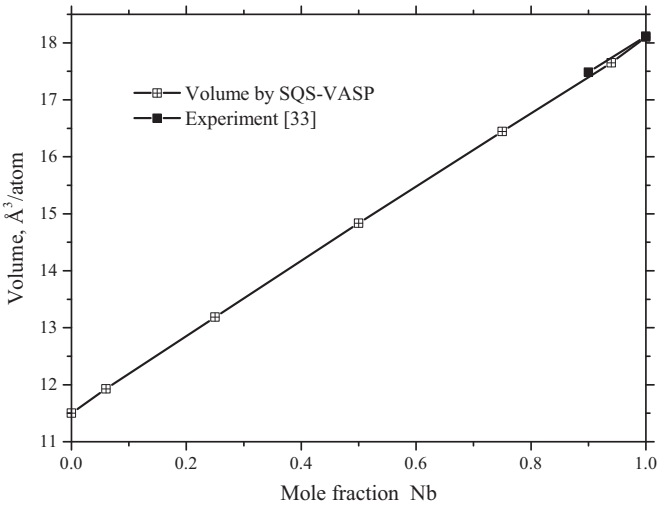

Fig. 2. The calculated volume of bcc in the Cr–Nb system by SQS-VASP compared with experimental data.

used to automatically generate input files for VASP calculations [11].

Special quasirandom structures (SQSs) are available for studying physical properties for solution phases depending on the correlation functions [12–14]. The structures are adequate representation of a random alloy when the correlation functions of the SQS and a fully random structure are approximately equal for the first several nearest neighbor shells. The enthalpies of mixing were obtained through the SQS-VASP approach using 16 atoms in the present work. The correlation functions of the structures, which were generated in Refs. [12–14] and adopted in the present work, represent a satisfactory match of fully random structures. The enthalpy of formation can be calculated from the first-principles calculation results as follows:

$$\Delta_f H_{AxBy} = E_{AxBy} - \left(\frac{x}{x+y}E_A + \frac{y}{x+y}E_B\right), \quad (1)$$

where the E_{AxBy}, E_A, E_B are the total energies obtained from the first-principles calculations for a compound or solution phase A_xB_y and the corresponding pure elements A and B. The x and y are the number of atoms of A and B in a structure.

In order to assess the ternary Zr–Nb–Cr system, the total energies of all end-member compounds modeling the Laves phases in the Cr–Nb and Zr–Cr as well as the Zr–Nb system were calculated.

3.2. Phonon calculations

In addition to the ground state calculations at 0 K, we performed the phonon calculations in order to obtain the energies at finite temperatures. In the present work, the calculations were carried out by supercell method [15] as implemented in ATAT code [16], with VASP as the computational engine. Supercells with 48 atoms and 96 atoms were used for the C15–$NbCr_2$ and C14–$NbCr_2$ structures, respectively. Displacement of 0.1 Å was adopted in the perturbed supercells. A 6*6*6 Gamma k-point mesh was used in the present work. The cutoff range of 7 Å was applied to fit the force constants by ATAT after VASP calculations. The phonon calculations were performed for the stoichiometric C14 and C15 Laves phases at 66.7 at% Cr (i.e. C14–$NbCr_2$ and C15–$NbCr_2$. Note that in the present work, we use C14–$NbCr_2$ et al. to denote stoichiometric compounds while C14 to denote the C14 Laves phase with solubility range) and the phase stability can be determined at finite temperatures.

3.3. CALPHAD modeling

As mentioned above, the CALPHAD method requires the modeling of the Gibbs energy of each phase as a function of temperature and pressure, and then all other thermodynamic properties can be obtained through thermodynamic correlations. In addition, phase equilibria and phase stabilities can also be calculated. In the following part we present the phenomenological models used in the present work.

At constant pressure, the relation between Gibbs energy and temperature for pure element i can be described as:

$$G_i - H^{SER}_{i,298.15} = a + bT + cT\ln T + dT^2 + eT^3 + fT^{-1} + gT^7 + hT^{-9}, \quad (2)$$

where $H^{SER}_{i,298.15}$ is the molar enthalpy of element i at 298.15 K and atmospheric pressure in its SER (Stable Element Reference) state, i.e. bcc for Nb and Cr, hcp for Zr. The parameters a to h are fitting values. The data of pure elements were taken from the SGTE compilation by Dinsdale [17].

3.3.1. Solution phases

In the Zr–Nb–Cr system, molar Gibbs energies of four solution phases, i.e. liquid, bcc, fcc and hcp, are described by the following expression:

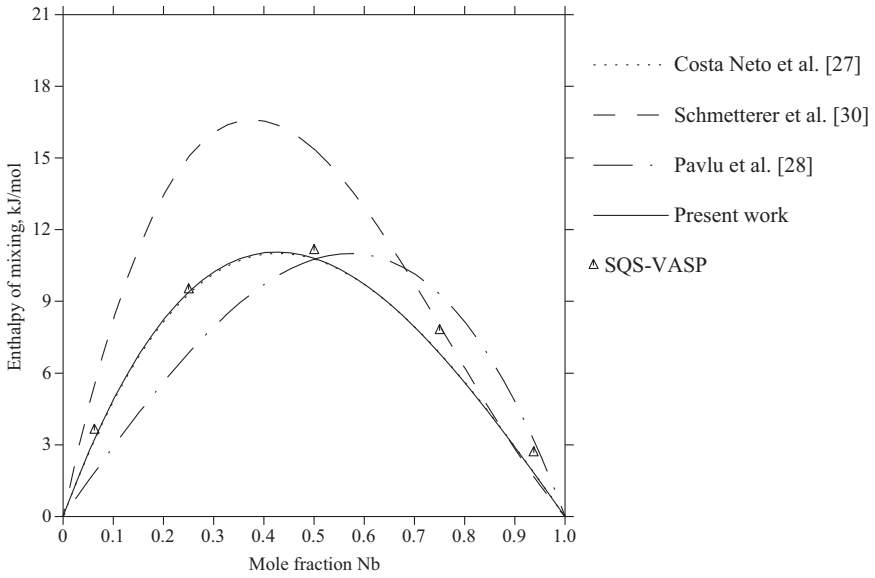

Fig. 3. Assessed enthalpy of mixing of bcc in the Cr–Nb system compared with SQS-VASP calculations and previous assessments.

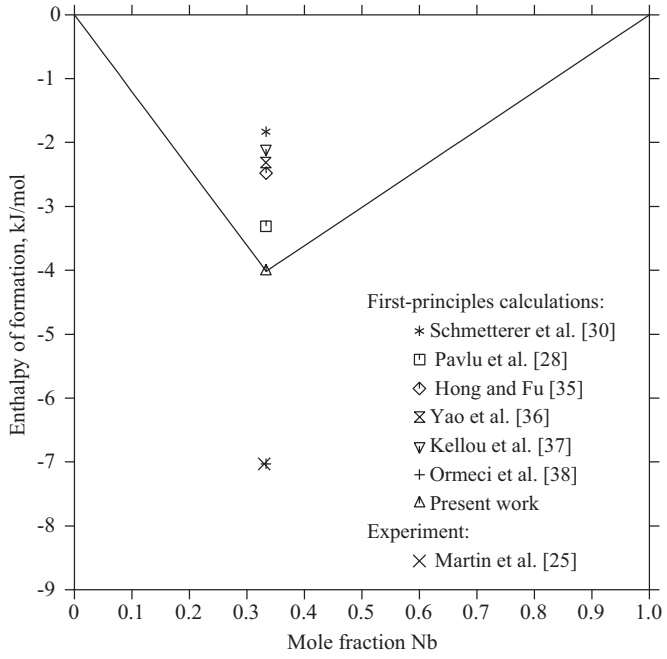

Fig. 4. Assessed enthalpy of formation of the C15 phase in the Cr–Nb system at 298 K compared with different first-principles calculations and experimental data. The reference states are bcc Cr and Nb.

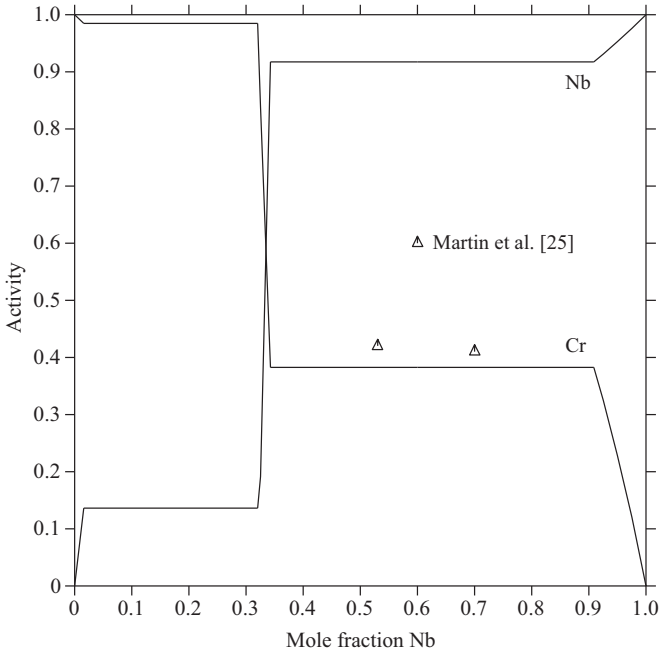

Fig. 5. The calculated activities of Cr and Nb at 1472 K in the Cr–Nb system compared with experimental data.

$$G = G^{ref} + \Delta G^{id}_{mix} + G^{E} + G^{mg}, \tag{3}$$

where $G^{ref} = \sum x_i G_i^0$ means the contribution of the mechanical mixing of pure elements to the total Gibbs energy, i represents pure element Zr, Nb or Cr. ΔG^{id}_{mix} is the ideal entropy of mixing. The excess Gibbs free energy, G^E, describes the deviation from the ideal solution. Take the Zr–Nb–Cr system for example, the formulae are given as

$$\Delta G^{id}_{mix} = RT(x_{Zr} \ln x_{Zr} + x_{Nb} \ln x_{Nb} + x_{Cr} \ln x_{Cr}) \tag{4}$$

$$G^{E} = x_{Zr}x_{Nb}\Omega_{ZrNb} + x_{Zr}x_{Cr}\Omega_{ZrCr} + x_{Nb}x_{Cr}\Omega_{NbCr} + x_{Zr}x_{Nb}x_{Cr}\Omega_{ZrNbCr}, \tag{5}$$

where R is the gas constant, T is the temperature. x_{Zr}, x_{Nb}, x_{Cr} represents the mole fraction of Zr, Nb and Cr. The interaction parameter of component i and j, Ω_{ij}, is expressed by the Redlich–Kister polynomial. G^{mg} denotes the magnetic contribution to the Gibbs energy. For pure Cr, the magnetic contribution to the Gibbs energy is obtained from the SGTE compilation by Dinsdale [17]. However, there is no interaction parameter needed for the magnetic contribution for the systems considered in the present work.

3.3.2. Intermetallic compounds

There are three types of intermetallic compounds, i.e. C14, C15 and C36 Laves phases. For the sake of simplicity and consistency with the multi-component databases, a two-sublattice model for

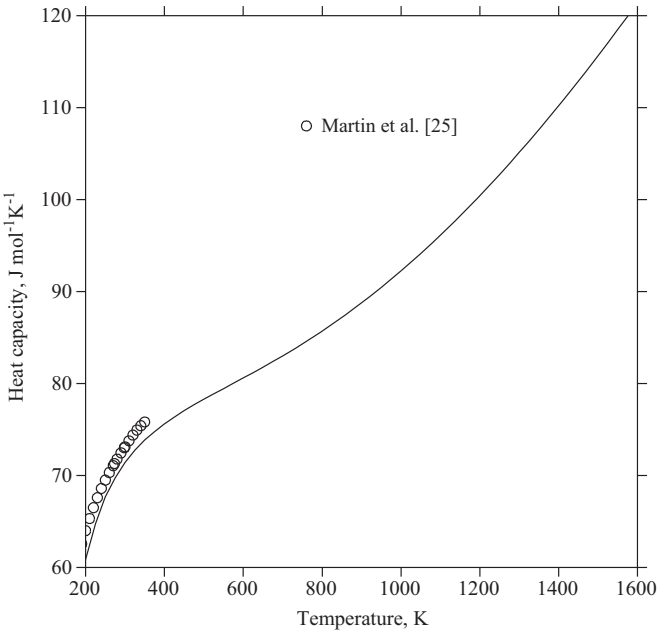

Fig. 6. Assessed heat capacity of C15–$NbCr_2$ compared with experimental data.

all Laves structures, $(A, B)_2(A, B)$, was adopted in order to describe their off-stoichiometric extension. Take ternary C15 phase for example, the model is $(Zr, Nb, Cr)_2(Zr, Nb, Cr)$ and the Gibbs energy can also be formulated by Eq. (3), but G^{ref}, ΔG^{id}_{mix} and G^E are expressed differently compared with Eqs (4–5):

$$G^{ref} = y'_{Zr}y''_{Zr}G_{Zr:Zr} + y'_{Zr}y''_{Cr}G_{Zr:Cr} + y'_{Zr}y''_{Nb}G_{Zr:Nb} + y'_{Nb}y''_{Nb}G_{Nb:Nb} + y'_{Nb}y''_{Zr}G_{Nb:Zr} + y'_{Nb}y''_{Cr}G_{Nb:Cr} + y'_{Cr}y''_{Nb}G_{Cr:Nb} + y'_{Cr}y''_{Zr}G_{Cr:Zr} + y'_{Cr}y''_{Cr}G_{Cr:Cr} \quad (6)$$

$$\Delta G^{id}_{mix} = RT[2*(y'_{Zr}\ln y'_{Zr} + y'_{Nb}\ln y'_{Nb} + y'_{Cr}\ln y'_{Cr}) + (y''_{ZR}\ln y''_{ZR} + y''_{Nb}\ln y''_{Nb} + y''_{Cr}\ln y''_{Cr}) \quad (7)$$

$$G^E = + y'_{Zr}y'_{Nb}(y''_{Zr}L_{Zr,Nb:Zr} + y''_{Nb}L_{Zr,Nb:Nb}) + y''_{Zr}y''_{Nb}(y'_{Zr}L_{Zr:Zr,Nb} + y'_{Nb}L_{Nb:Zr,Nb}) + y'_{Zr}y'_{Cr}(y''_{Zr}L_{Zr,Cr:Zr} + y''_{Cr}L_{Zr,Cr:Cr}) + y''_{Zr}y''_{Cr}(y'_{Zr}L_{Zr:Zr,Cr} + y'_{Nb}L_{Nb:Zr,Cr}) + y'_{Nb}y'_{Cr}(y''_{Nb}L_{Nb,Cr:Nb} + y''_{Cr}L_{Nb,Cr:Cr}) + y''_{Nb}y''_{Cr}(y'_{Cr}L_{Cr:Nb,Cr} + y'_{Nb}L_{Nb:Nb,Cr}), + y'_{Zr}y'_{Nb}y'_{Cr}(y''_{Zr}L_{Zr,Nb,Cr:Zr} + y''_{Nb}L_{Zr,Nb,Cr:Nb} + y''_{Cr}L_{Zr,Nb,Cr:Cr}) + y''_{Zr}y''_{Nb}y''_{Cr}(y'_{Zr}L_{Zr:Zr,Nb,Cr} + y'_{Nb}L_{Nb:Zr,Nb,Cr} + y'_{Cr}L_{Cr:Zr,Nb,Cr}) \quad (8)$$

where y'_i and y''_i denote the mole fraction of i in the first and second sublattice, L means the interaction parameter. There are nine stoichiometric end-member compounds in the model. One of them is described, for example, as:

$$G_{Cr_2Nb} = A + B*T + 2*G^{REF}_{Cr} + G^{REF}_{Nb} \quad (9)$$

The constant A represents the enthalpy of formation obtained from Eq. (1), the term $B*T$ concerns the entropy contribution to the Gibbs energy. G^{SER}_{Cr} and G^{SER}_{Nb} are the Gibbs energies of Cr and Nb, respectively, adopting the SER reference state. Eq. (9) follows the Kopp–Neuman law stating that the heat capacity of a solid compound is approximately a linear average of its constituent components weighted by its composition.

Table 3
Assessed thermodynamic parameters of the Zr–Nb–Cr system. The SGTE values of pure elements (GHSERZR, GHSERNB and GHSERCR) are taken from Dinsdale [17].

Phases	Parameters
Liquid	$L_{Cr,Nb:VA;0} = -11204.0 - 0.61*T$
	$L_{Cr,Nb:VA;1} = -8513.4 - 0.50*T$
	$L_{Cr,Zr;0} = -10071.3 + 1.20*T$
	$L_{Cr,Zr;1} = -1425.9 - 0.74*T$
	$L_{Cr,Zr;2} = -8284.8 + .92*T$
	$L_{Nb,Zr;0} = 10311.0$ [52]
	$L_{Nb,Zr;1} = 6709.0$ [52]
	$L_{Cr,Nb,Zr;0} = 16800.0$
Bcc	$L_{Cr,Nb:VA;0} = 43600.0 - 13.60*T$
	$L_{Cr,Nb:VA;1} = 13755.2 - 6.80*T$
	$L_{Cr,Zr;0} = 48365.4 - 13.90*T$
	$L_{Cr,Zr;1} = 10065.5 - 6.10*T$
	$L_{Nb,Zr;0} = 15911.0 + 3.35*T$ [52]
	$L_{Nb,Zr;1} = 3919.0 - 1.09*T$ [52]
	$L_{Cr,Nb,Zr;0} = 54600.0$
	$L_{Cr,Nb,Zr;1} = -18200.0$
	$L_{Cr,Nb,Zr;2} = 69500.0$
Hcp	$L_{Cr,Zr;0} = 89700.0 - 11.00*T$
	$L_{Cr,Zr;1} = 38800.0 + 6.00*T$
	$L_{Nb,Zr;0} = 24411.0$ [52]
	$L_{Cr,Nb,Zr;0} = 64500.0$
C15 $(Zr,Cr,Nb)_2(Zr,Cr,Nb)$	$G_{Zr:Zr} = 81154.0 - 8.33*T + 3*GHSERZR$
	$G_{Cr:Cr} = 79374.0 - 2.59*T + 3*GHSERCR$
	$G_{Nb:Nb} = 48976.0 + 0.31*T + 3*GHSERNB$
	$G_{Cr:Nb} = -12051.0 - 6.98*T + 2*GHSERCR + GHSERNB$
	$G_{Nb:Cr} = 213353.0 - 7.65*T + GHSERCR + 2*GHSERNB$
	$G_{Nb:Zr} = 13904.0 + 9.40*T + GHSERZR + 2*GHSERNB$
	$G_{Zr:Nb} = 145110.0 + 9.00*T + GHSERNB + 2*GHSERZR$
	$G_{Cr:Zr} = -13971.1 - 9.22*T + 2*GHSERCR + GHSERZR$
	$G_{Zr:Cr} = 303085.2 - 8.46*T + GHSERCR + 2*GHSERZR$
	$L_{Cr,Nb:Nb} = 50900.0$
	$L_{Cr:Cr,Nb} = -40400.0$
	$L_{Cr,Zr:Zr} = 16850.0$
	$L_{Cr:Cr,Zr} = -16500.0$
	$L_{Cr:Zr,Cr,Nb} = -93650.0$
C36 $(Zr,Cr,Nb)_2(Zr,Cr,Nb)$	$G_{Zr:Zr} = 69218.7 - 3.44*T + 3*GHSERZR$
	$G_{Cr:Cr} = 77859.0 - 6.33*T + 3*GHSERCR$
	$G_{Nb:Nb} = 48330.0 - 0.36*T + 3*GHSERNB$
	$G_{Cr:Zr} = -11809.8 - 10.40*T + 2*GHSERCR + GHSERZR$
	$G_{Zr:Cr} = 228202.8 - 8.51*T + GHSERCR + 2*GHSERZR$
	$G_{Zr:Nb} = 131310.0 + 1.00*T + GHSERNB + 2*GHSERZR$
	$G_{Nb:Zr} = 9098.6 + 9.00*T + GHSERZR + 2*GHSERNB$
	$G_{Cr:Nb} = -10517.0 + 1.00*T + 2*GHSERCR + GHSERNB$
	$G_{Nb:Cr} = 216420.0 + 1.00*T + GHSERCR + 2*GHSERNB$
	$L_{Cr,Zr:Zr} = 19750.0$
	$L_{Cr:Cr,Zr} = -9540.0$
C14 $(Zr,Cr,Nb)_2(Zr,Cr,Nb)$	$G_{Zr:Zr} = 62388.0 - 4.32*T + 3*GHSERZR$
	$G_{Cr:Cr} = 83339.0 - 2.30*T + 3*GHSERCR$
	$G_{Nb:Nb} = 46538.0 + 3*GHSERNB$
	$G_{Cr:Zr} = -9050.3 - 11.85*T + 2*GHSERCR + GHSERZR$
	$G_{Zr:Cr} = 279176.1 - 4.32*T + GHSERCR + 2*GHSERZR$
	$G_{Zr:Nb} = 123440.0 + 8.00*T + GHSERNB + 2*GHSERZR$
	$G_{Nb:Zr} = 4833.9 + 8.00*T + 2*GHSERNB + GHSERZR$
	$G_{Nb:Cr} = 21699.0 + 9.00*T + 2*GHSERNB + GHSERCR$
	$G_{Cr:Nb} = -7728.5 + 9.00*T + 2*GHSERCR + GHSERNB$
	$L_{Cr,Zr:Zr} = 27800.0$
	$L_{Cr:Cr,Zr} = -22800.0$

4. Results and discussion

4.1. Cr–Nb system

There are four phases, i.e. liquid, bcc, C15 and controversial C14 in the Cr–Nb binary system. Phase equilibria of the Cr–Nb system have been investigated by many researchers experimentally. Elyutin and Funke [18] determined the solid phase boundaries. The temperatures and liquid compositions of the invariant reactions were also measured [19–21]. Zakharova and Prokoshkin [22] determined the phase boundaries of Laves phases and solution

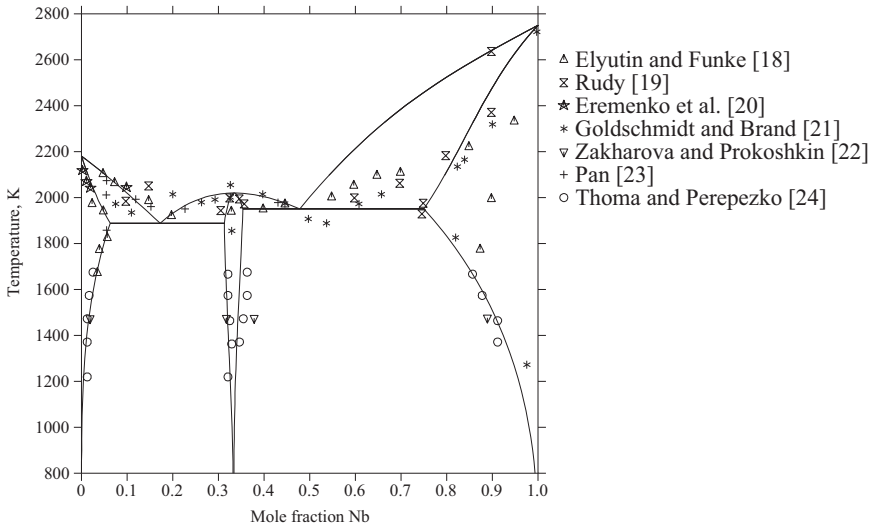

Fig. 7. The calculated Cr–Nb phase diagram compared with experimental data (all data represent phase boundaries).

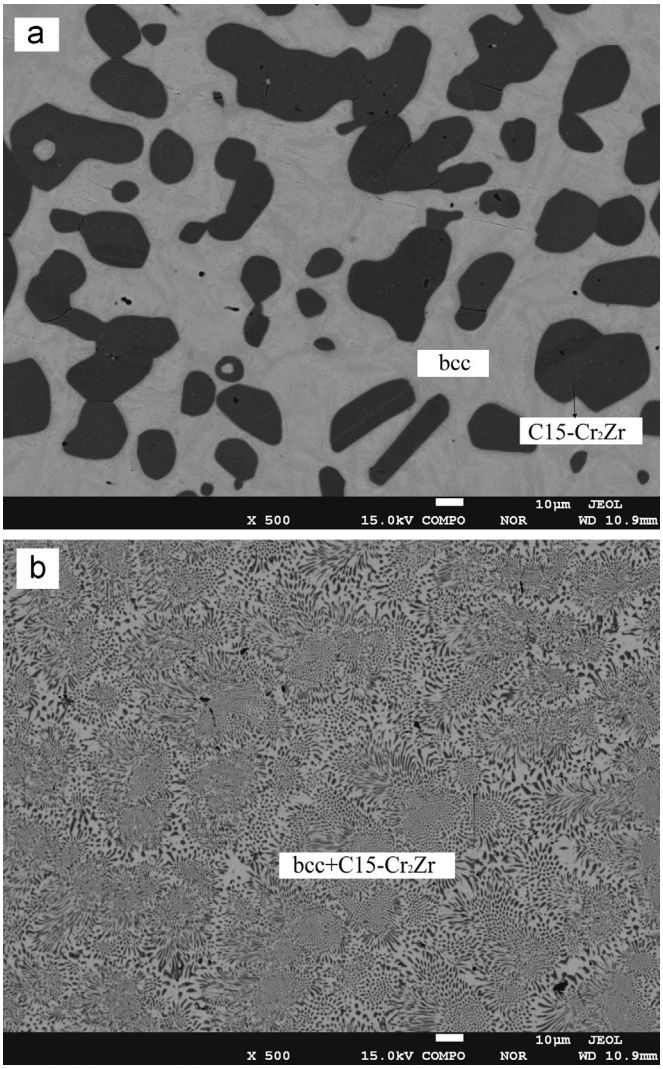

Fig. 8. BSE images of the 1273 K annealed samples for (a) Cr–60 at% Zr (b) Cr–20 at% Zr.

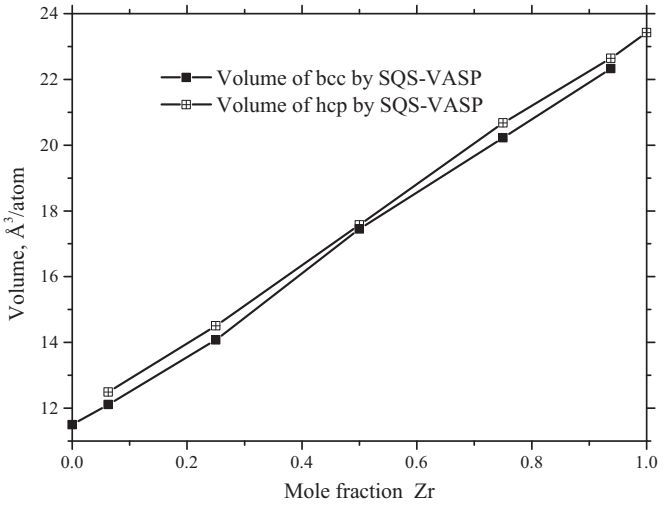

Fig. 9. The calculated volume of bcc and hcp phases in the Zr–Cr system by SQS-VASP.

phases. Pan [23] reported the existence of C14 phase at above 1858 K for the first time. Thoma and Perepezko [24] confirmed its existence between 1858 K and 2003 K based on the analysis of X-ray patterns. Martin et al. [25] determined the specific heats and activities by calorimetry and calculated the enthalpy of formation and entropy of formation of C15–$NbCr_2$ at 298.15 K as −7 kJ/mol and −0.2 J/K/mol, respectively. Venkatranman and Neumann [26] summarized the literature data for this system. Costa Neto et al. [27] performed a thermodynamic assessment based on the aforementioned experimental data. Pavlů et al. [28] reassessed the Laves phases in the system using the first-principles results at 0 K. To better fit the phase diagram, they evaluated the entropy values of several end-member compounds.

All data mentioned above were considered in the present assessment. There appears to be a consistent trend with the data from Elyutin and Funke [18], Goldschmidt and Brand [21] and Rudy [19]. However, as we accept the thermodynamic description of Nb by Dinsdale [17] and to be consistent within a multi-component database, it was not intended to fit all the liquidus and solidus data in the present work.

Recently, Aufrecht et al. [29] pointed out that the high-temperature phase C14 considered as a stable phase was actually the η-carbide-type phase by experiments. The metastable C14 phase can be obtained by extremely fast cooling. In a more recent work,

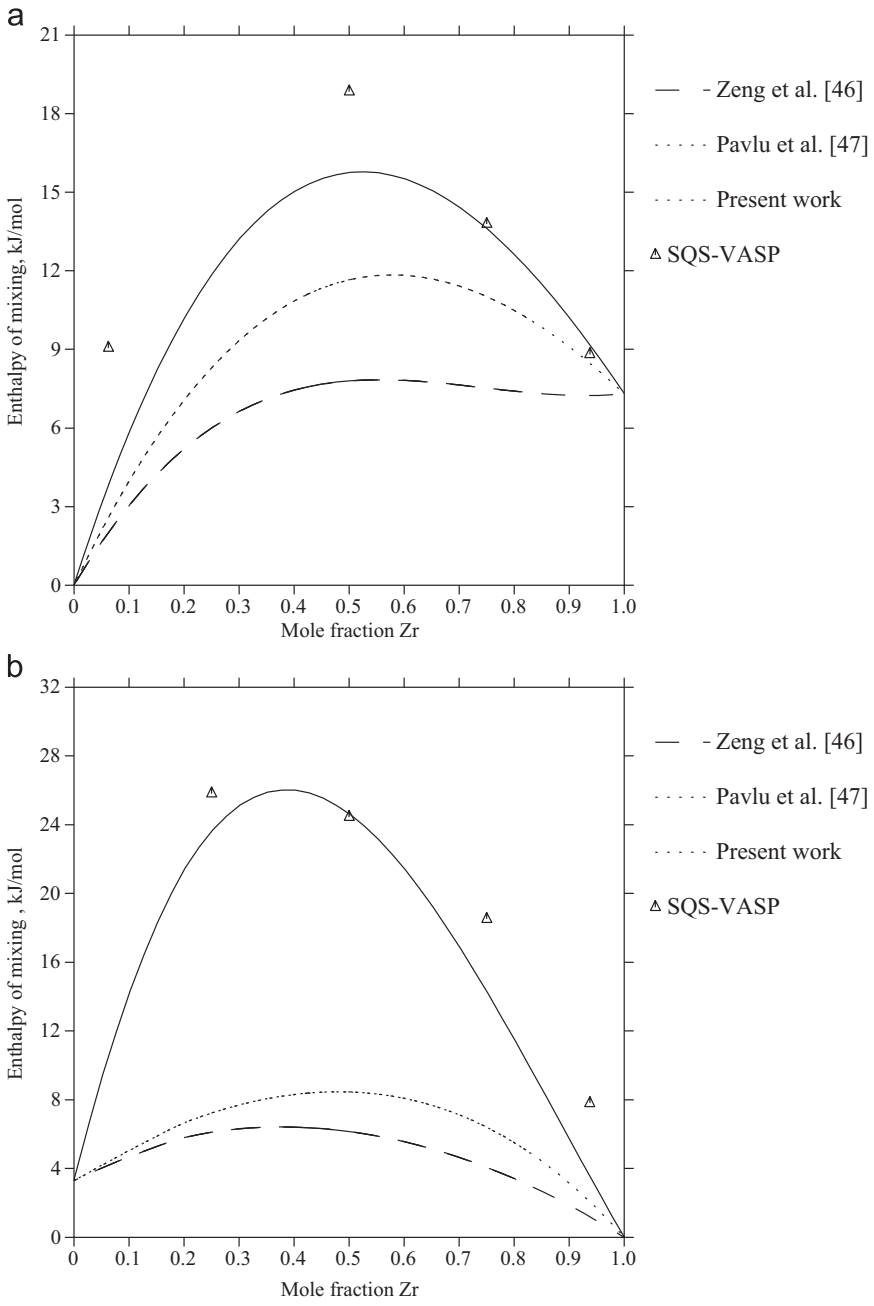

Fig. 10. Enthalpies of formation of bcc (a) and hcp (b) in the Zr–Cr system compared with SQS-VASP calculations and previous assessments.

Schmetterer et al. [30] analyzed the stability of C14 from several aspects. They accepted the viewpoint that the C14 structure is not stable and then presented a thermodynamic description of the Cr–Nb system without the C14 phase. One of the important argument that Schmetterer et al. hold was that the radius ratio ($r_{Nb}/r_{Cr}=1.148$) and the electron concentration (between 5.61 and 5.7 [31,32]) seem more likely to favor the formation of the C15 phase, but it cannot be ruled out that C14 is metastable at high temperatures theoretically. Therefore, in the present work, we studied the stability of C14 from the perspective of the first-principles calculations, especially phonon calculations. According to Table 2, which lists the results of enthalpies of formation and lattice parameters of all stoichiometric Laves phases as well as the literature results from the ground state calculations, the enthalpies of formation for C15–$NbCr_2$ and C14–$NbCr_2$ are −4160 J/mol and −2577 J/mol, respectively. The results confirm the stability of C15–$NbCr_2$ phase at 0 K. Furthermore, the phonon calculations provided the Gibbs energy curve versus temperature. The Gibbs energy of C14–$NbCr_2$ is larger than that of C15–$NbCr_2$ in the whole temperature range. In other words, the Gibbs energy difference showing in Fig. 1(a), $\Delta G^{C14\rightarrow C15} = \Delta G^{C15} - \Delta G^{C14}$, keeps negative with increasing temperature. In this way we prove that the C14–$NbCr_2$ is metastable at all temperatures, which confirms the previous experimental work and analysis [29,30]. Therefore the C14 was treated as a metastable phase in the following assessment. For comparison, the same calculation was carried out for the stoichiometric C14–$ZrCr_2$ and C15–$ZrCr_2$ in the Zr–Cr system as shown in Fig. 1(b). The Gibbs energy of C14–$ZrCr_2$ is smaller than that of the C15–$ZrCr_2$ above 2071 K, above which $\Delta G^{C14\rightarrow C15}$ turns from negative to positive and the C14–$ZrCr_2$ should be a stable phase.

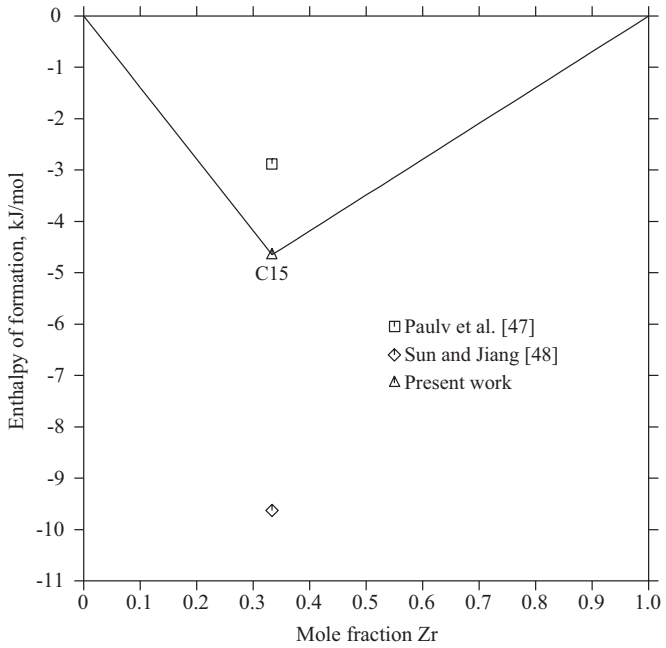

Fig. 11. Assessed enthalpy of formation of the C15 phase in the Zr–Cr system at 298 K compared with different first-principles calculations. The reference states are hcp Zr and bcc Cr.

The values from the first-principles calculations were used to consummate the thermodynamic description for bcc and Laves phase. Previous assessments [27,28,30] evaluated the enthalpies of solution phases mainly based on phase diagram data. In order to improve the thermodynamic description, we calculated the energy and volume of the bcc solution phase at 0 K in the present work. The calculated volume compared with experimental data [33] is shown in Fig. 2. The enthalpy of mixing was derived from Eq. (1) and adopted in the present assessment. The enthalpy of mixing of the bcc phase from previous assessments as well as the SQS-VASP results is shown in Fig. 3. As seen from the figure, the present assessment provides a description of the bcc phase that is more consistent with the first-principles results than previous work [28,30]. The enthalpy of formation of the system at 298 K is presented in Fig. 4. All the first-principles calculated as well as the assessed values are considerably larger than the experimental data. The enthalpy value from the present work is the lowest among all the first-principles calculation results and the closest to the experimental data.

The constant terms of the model parameters for the end-member compounds of the Laves phases were obtained from the first-principles calculations at 0 K, and the temperature coefficients were assessed to fit various aforementioned experimental data. As the solid phases were reassessed, the parameters of liquid were modified based on the previous work [27] in order to fit the phase diagram.

The calculated activities of Cr at 1472 K in Fig. 5 is in line with the data from Martin et al. [25], which is 0.41 and 0.42 at the composition of 70 at% and 53 at% Cr, respectively. The assessed heat capacity comparing with experimental data [25] presented in Fig. 6 shows the feasibility of the model for C15, which follows the Kopp–Neuman law close to the room temperature.

The thermodynamic parameters describing the Cr–Nb system are listed in Table 3. The calculated phase diagram in Fig. 7 shows a good agreement with the available experimental data except for the liquidus and solidus in the Nb-rich region.

4.2. Zr–Cr system

Domagala et al. [39] determined the phase equilibrium of the Zr–Cr system, and subsequently revised the temperature of the Cr-rich eutectic. Further on, Gebhardt et al. [40] measured the liquidus and the solubility of Zr in bcc Cr. Rumball and Elder [41] determined the eutectic reaction temperature of bcc to hcp Zr and C15–$ZrCr_2$ transformation as 1108 K. Petkov et al. [42] reported the phase boundaries and transformation temperature of Laves phases using high-temperature X-ray technique, and found that the C36 structure existed. Nemoshkalenko et al. [43] studied the phase boundary of Laves phases. Shen and Paesche [44] investigated that the temperature that $ZrCr_2$ transformed from C15 to C14 was between 1823 K and 1873 K. Arias and Abriata [45] constructed an assessed phase diagram based on the experimental results mentioned above.

Taking the thermodynamic data into consideration, Zeng and Hämäläinen [46] presented a thermodynamic model of the Laves phases in the Zr–Cr system. Recently Pavlů et al. carried out the first-principles calculations on the total energies of Laves phases in all three structures, i.e. C14, C15 and C36 [47]. Then they derived a thermodynamic description of the Zr–Cr system based on the calculation results.

In the present work, two alloys were annealed at different temperatures to determine the phase boundary related to the C15 Laves phase, especially on the Cr-rich part. The alloys show similar two-phase microstructure at different temperatures. Backscattered electron (BSE) image of the alloys annealed at 1273 K are given in Fig. 8. Fig. 8(a) shows two contrasts, grey and dark, representing the bcc and C15 Laves phase respectively, which is opposite in Fig. 8(b). The compositions determined by EPMA are listed in Table 1, which were employed in the present thermodynamic assessment. For the alloy with 20 at% Zr, the dark bcc grain is generally fine and difficult for EPMA measurements. However, it is possible to find large particles ($>2\ \mu m$) with the diameter larger than the electron beam spot diameter ($<1\ \mu m$) for EPMA used in the present work. The EPMA measurements were performed at several different positions and the results are almost the same. The present experimental data shows good agreement with previous results [39–41], which were adopted for the assessment. The experimental results related to the Laves phases from Petkov et al. [42] and Nemoshkalenko et al. [43] were used to for the assessment.

The total energies of all end-member compounds modeling Laves phases were calculated, and the SQS calculations were performed to obtain the enthalpies of mixing of bcc and hcp solution phases at different compositions at 0 K. The result shown in Fig. 9 indicates that the variation of calculated volume with composition follows the Vegard law. The interaction parameters of solution phases listed in Table 3 were optimized based on enthalpies of mixing from SQS-VASP calculations. The calculated enthalpies of mixing for bcc and hcp solution phases in Fig. 10 are in considerably better agreement with the first-principles calculated formation enthalpies than previous works [46,47]. The results of the first-principles calculations were employed in the assessments of end-member compounds to describe the enthalpies of intermetallic compounds. Fig. 11 shows the enthalpy of formation of the system calculated from the optimized database compared with the first-principles calculations from different researchers [47,48].

Based on all these results, we reassessed the interaction parameters of solution phases firstly. The parameters of end-members in the Laves phases were based on the first-principles calculations, the temperature coefficient were optimized to fit the phase diagram. The thermodynamic parameters describing the Zr–Cr system are listed in Table 3. The model described in Section 3.3.2 provides a good description of the system. The calculated phase

diagram in Fig. 12 with experimental data shows the accuracy of the thermodynamic description. The calculated phases region of bcc and C15 Laves phase was narrower compared to the previous work [46,47] based on the present experimental data.

4.3. Zr–Nb–Cr system

The published experimental result of the ternary system is comparatively scarce. Kornilov et al. [50] determined the isopleth of $NbCr_2$–$ZrCr_2$, which were not employed in the present assessment as the C36 phase was not considered. Kim and Takasugi [51] measured the isothermal section at 1573 K. Combining with the assessment of Zr–Nb system by Guillermet [52], the thermodynamic description of Zr–Nb–Cr system was established based on the isothermal section and the first-principle calculations for the Laves phases in the Zr–Nb system. The parameters in the ternary system are listed in Table 3. The calculated isothermal section at 1573 K in Fig. 13 shows a good agreement with the experimental data [51].

5. Conclusion

The phonon calculations of both C14 and C15 structures of the stoichiometric $NbCr_2$ phase confirmed the metastability of C14–$NbCr_2$ at high temperatures. In contrast, the C14–$ZrCr_2$ is stable at high temperatures according to the calculation results. The thermodynamic descriptions of the Cr–Nb and Zr–Cr with extension to the ternary Zr–Nb–Cr system were established based on the available data. The enthalpies of formation of the end-member compounds for Laves phases as well as the solution phases agree well with the first-principles calculations. To remain consistent with the present experimental results, the calculated single-phase regions of bcc and C15 phases in the Zr–Cr system are smaller comparing to the previous assessments [46,47]. With the present optimized parameters, various phase equilibrium and thermodynamic properties can be obtained for the Zr–Nb–Cr system.

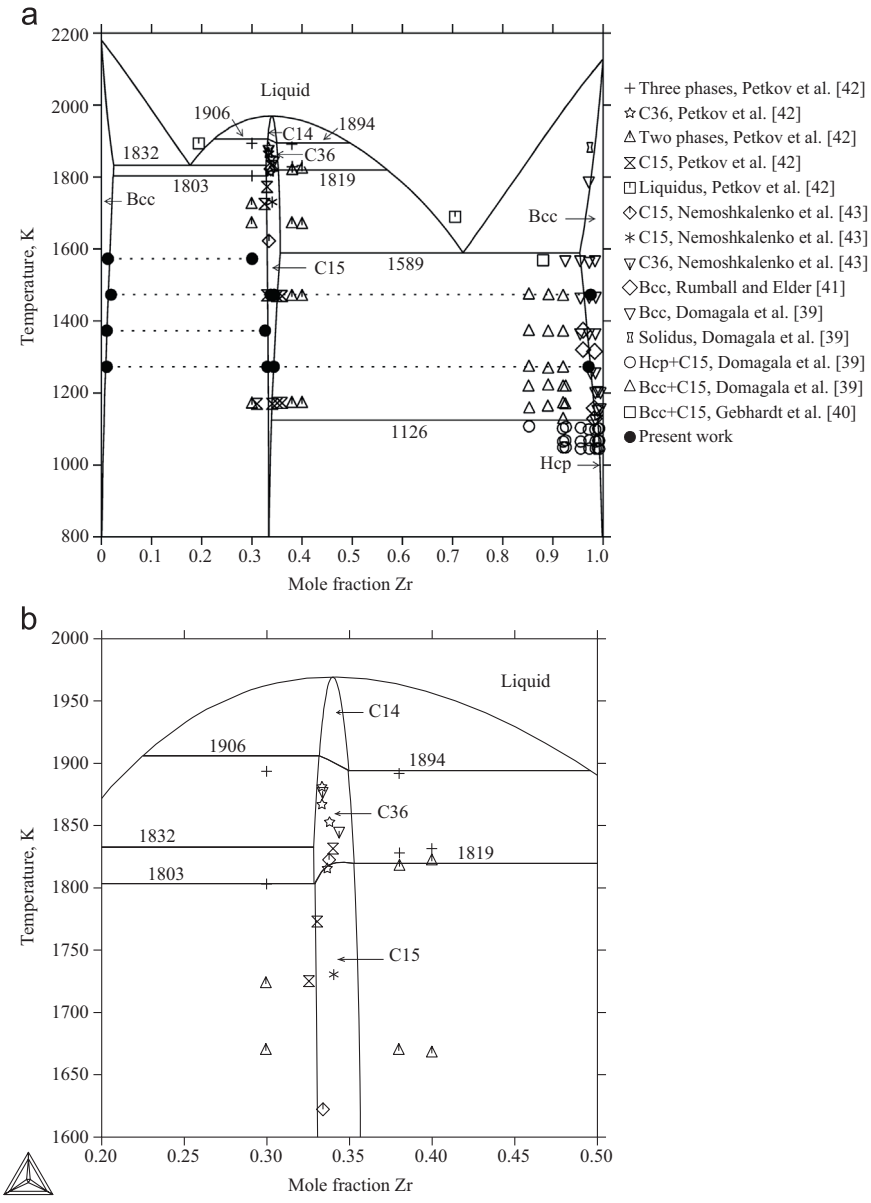

Fig. 12. The Calculated Zr–Cr phase diagram compared with experimental data. Fig. (b) is the enlarged part of (a) showing the detailed phase quilibria of Laves phases.

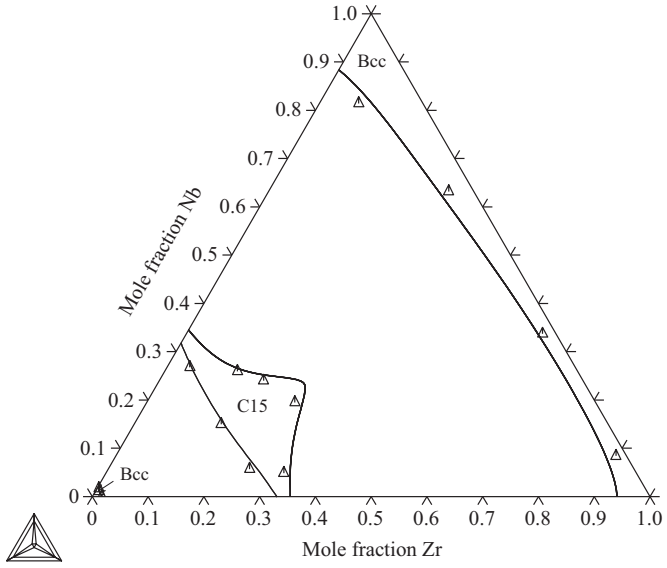

Fig. 13. Assessed isothermal section at 1573 K compared with experimental data [51].

Acknowledgements

The authors gratefully acknowledge the financial supports from the Shanghai Oriental Scholarship and the financial support from the National Key Project of Science and Technology (Grant number: 2012ZX06004-012).

Appendix A. Supplementary material

Supplementary data associated with this article can be found in the online version at http://dx.doi.org/10.1016/j.calphad.2015.06.002.

References

[1] M. Griffiths, J. Nucl. Mater. 159 (1988) 190–218.
[2] B. Cox, J. Nucl. Mater. 336 (2005) 331–368.
[3] S.J. Zinkle, G.S. Was, Acta Mater. 61 (2013) 735–758.
[4] N. Saunders, A.P. Miodownik, CALPHAD, Elsevier, London, 1998.
[5] H.L. Lukas, S.G. Fries, B. Sundman, Computational Thermodynamics: The Calphad Method, Cambridge University Press, Cambridge, 2007.
[6] D.J. Singh, Planewaves, Pseudopotentials and the LAPW Method, Kluwer, Boston, 1994.
[7] G. Kresse, J. Furthmüller, Comp. Mater. Sci. 6 (1996) 15–50.
[8] G. Kresse, J. Furthmüller, Phys. Rev. B 54 (1996) 11169–11186.
[9] G. Kresse, J. Joubert, Phys. Rev. B 59 (1999) 1758–1775.
[10] J.P. Perdew, Y. Wang, Phys. Rev. B 45 (1992) 13244–13249.
[11] J.C. Crivello, A. Breidi, J.M. Joubert, Inorg. Chem. 52 (2013) 3674–3686.
[12] C. Jiang, C. Wolverton, J. Sofo, L.Q. Chen, Z.K. Liu, Phys. Rev. B 69 (21) (2004) 214202.
[13] D. Shin, R. Arróyave, Z.K. Liu, Phys. Rev. B 74 (2) (2007) 144204.
[14] S.H. Wei, L.G. Ferreira, J.E. Bernard, A. Zunger, Phys. Rev. Lett. 65 (1990) 353–356.
[15] A. van de Walle, G. Ceder, Rev. Mod. Phys. 74 (2002) 11–45.
[16] A. van de Walle, M. Asta, G. Ceder, CALPHAD 26 (2002) 539–553.
[17] A.T. Dinsdale, CALPHAD 15 (1991) 317–425.
[18] V.P. Elyutin, V.F. Funke, Izv. Acad. Nauk SSSR Otd. Tekh. Nauk 3 (1956) 68–76.
[19] E. Rudy, Technical Report AFML-TR-65-2, 21, 1969, 127–130.
[20] V.N. Eremenko, G.V. Zudilova, L.A. Gaevskayam, Metalloved. I, Obrabotka Met. 1 (1958) 11–16.
[21] H.J. Goldschmidt, J.A. Brand, J. Less Common Met. 3 (1961) 44–61.
[22] M.I. Zakharova, D.A. Prokoshkin, Izv. Akad. Nauk SSSR, Met. i Topl. 4 (1961) 59.
[23] V.M. Pan, Fiz. Met. Metalloved. 12 (1961) 455–457.
[24] D.J. Thoma, J.H. Perepezko, Mater. Sci. Eng. 156 (1992) 97–108.
[25] J.F. Martin, F. Müller, O. Kubaschewski, Trans. Faraday Soc. 66 (1970) 1065–1072.
[26] M. Venkatraman, J.P. Neumann, Bull. Alloy Phase Diagr. 7 (1986) 462–466.
[27] J.G. Costa Neto, S.G. Fries, H.L. Lukas, S. Gama, G. Effenberg, CALPHAD 17 (1993) 219–228.
[28] J. Pavlů, J. Vřeštal, M. Šob, CALPHAD 33 (2009) 179–186.
[29] J. Aufrecht, A. Leineweber, A. Senyshyn, E.J. Mittemeijer, Scr. Mater. 62 (2010) 227–230.
[30] C. Schmetterer, A. Khvan, A. Jacob, B. Hallstedt, T. Markus, J. Phase Equilib. Diff. 35 (2014) 434–444.
[31] J.H. Zhu, P.K. Liaw, C.T. Liu, Mater. Sci. Eng. A 239–240 (1990) 260–264.
[32] J.H. Zhu, C.T. Liu, L.M. Pike, P.K. Liaw, Metall. Mater. Trans. A 30A (1999) 1449–1452.
[33] H. Rassaerts, F. Benesovsky, H. Nowotny, Planseeber. f. Pulvermetall. 13 (1965) 199–206.
[34] V. Blazina, R. Trojko, J. Less-Common Met. 119 (1986) 297–305.
[35] S. Hong, C.L. Fu, Intermetallics 7 (1999) 5–9.
[36] Q. Yao, J. Sun, Y. Zhang, B. Jiang, Acta Mater. 54 (2006) 3585–3591.
[37] A. Kellou, T. Grosdidier, C. Coddet, H. Aourag, Acta Mater. 53 (2005) 1459–1466.
[38] A. Ormeci, F. Chu, J. Wills, J.M. Wills, T.E. Mitchell, R.C. Albers, D.J. Thoma, S. P. Chen, Phys. Rev. B 54 (18) (1996) 12753–12762.
[39] R.F. Domagala, D.J. McPherson, M. Hansen, Trans. AIME 197 (1953) 279–283.
[40] E. Gebhardt, J. Rexer, G. Petzow, Z. Metallkd. 58 (1967) 534–541.
[41] W.M. Rumball, F.G. Elder, J. Less-Common Met. 19 (1969) 345–358.
[42] V.V. Petkov, S.B. Prima, L.A. Tretyatchenko, Yu.A. Kocherzhinskii, Metallofiz. 46 (1973) 80–84.
[43] V.V. Nemoshkalenko, A.P. Nesenyuk, V.P. Krivitskii, V.V. Petkov, L.I. Nikolaev, A. V. Polenur, B.P. Memko., A.P. Spak, M.A. Midlina, R.K. Ostafiichuk, Metallofiz. 52 (1974) 54–58.
[44] Y.S. Shen, O.G. Paesche, Trans. AIME 242 (1968) 2241–2242.
[45] D. Arias, J.P. Abriata, Bull. Alloy Phase Diagr. 7 (1986) 237–243.
[46] K. Zeng, M. Hämäläinen, K. Lilius, CALPHAD 17 (1993) 101–107.
[47] J. Pavlů, J. Vřeštal, M. Šob, CALPHAD 33 (2009) 382–387.
[48] J. Sun, B. Jiang, Philos. Mag. 84 (2004) 3133–3144.
[49] S. Hirosawa, F. Pourarian, V.K. Sinha, W.E. Wallace, J. Magn. Magn. Mater. 38 (1983) 159–164.
[50] I.I. Kornilov, S.P. Alisova, P.B. Budberg, Inorg. Mater. 1 (1965) 1993–1995.
[51] W.Y. Kim, T. Takasugi, Scr. Mater. 48 (2003) 559–563.
[52] A.F. Guillermet, Z. Metallkd. 82 (1991) 478–487.